Volume 6 • Number 5 May 2006

www.aspbs.com/jnn

Journal of NANOSCIENCE and NANOTECHNOLOGY

Editor-in-Chief: Hari Singh Nalwa, USA

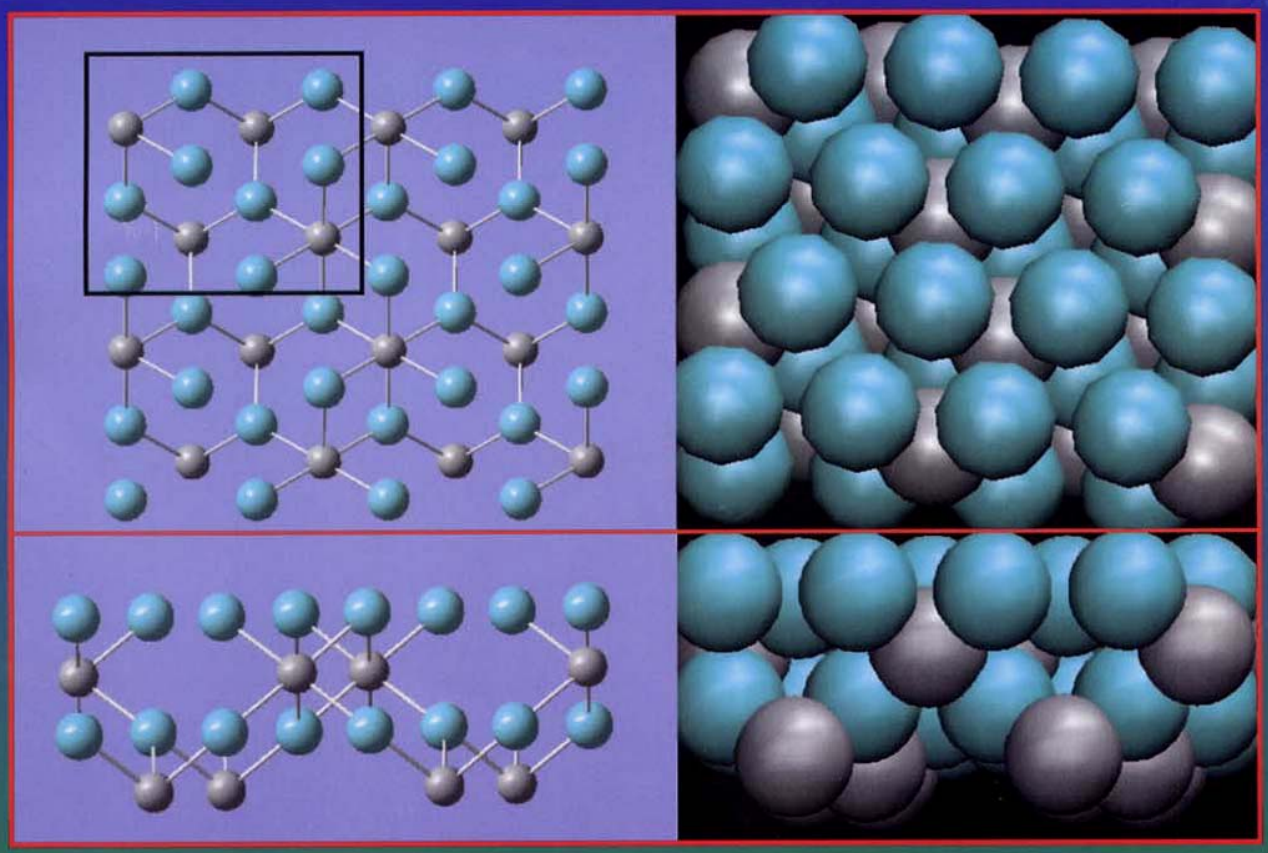

A Special Issue on

SWCNT Growth Mechanisms

GUEST EDITOR: Sivaram Arepalli

ASP
AMERICAN SCIENTIFIC PUBLISHERS

Journal of
Nanoscience and Nanotechnology
Vol. 6, 1416–1422, 2006

Sol–Gel Fabrication and Photoluminescence Properties of SiO_2@Gd_2O_3:Eu^{3+} Core–Shell Particles

G. Z. Li,[1,2] M. Yu,[1,2] Z. L. Wang,[1] J. Lin,[1,*] R. S. Wang,[2] and J. Fang[3]

[1] *Key Laboratory of Rare Earth Chemistry and Physics, Changchun Institute of Applied Chemistry, Chinese Academy of Sciences, Changchun 130022, P. R. China*
[2] *Department of Chemistry, Northeast Normal University, Changchun 130024, P. R. China*
[3] *Department of Chemistry and Advanced Materials Research Institute, University of New Orleans, New Orleans, Louisiana 70148, USA*

A uniform nanolayer of europium-doped Gd_2O_3 was coated on the surface of preformed submicron silica spheres by a Pechini sol–gel process. The resulted SiO_2@Gd_2O_3:Eu^{3+} core–shell structured phosphors were characterized by X-ray diffraction (XRD), Fourier transform infrared spectroscopy (FT-IR), field emission scanning electron microscopy (FESEM), transmission electron microscopy (TEM), photoluminescence (PL) spectra as well as kinetic decays. The XRD results show that the Gd_2O_3:Eu^{3+} layers start to crystallize on the SiO_2 spheres after annealing at 400 °C and the crystallinity increases with raising the annealing temperature. The core–shell phosphors possess perfect spherical shape with narrow size distribution (average size: 640 nm) and non-agglomeration. The thickness of the Gd_2O_3:Eu^{3+} shells on the SiO_2 cores can be adjusted by changing the deposition cycles (70 nm for three deposition cycles). Under short UV excitation, the obtained SiO_2@Gd_2O_3:Eu^{3+} particles show a strong red emission with $^5D_0$–$^7F_2$ (610 nm) of Eu^{3+} as the most prominent group. The PL intensity of Eu^{3+} increases with increasing the annealing temperature and the number of coating cycles.

Keywords: Gd_2O_3:Eu^{3+}, SiO_2, Core–Shell, Sol–Gel Process, Photoluminescence.

RESEARCH ARTICLE

1. INTRODUCTION

The core–shell particles have been attracting a great deal of interests due to their fantastic properties different from those of single-component materials, and their synthesis has opened new directions for material research.[1,2] Core–shell materials consist of a core structural domain covered by a shell domain. The core and shell domains may be composed of a variety of materials including polymers, inorganic solids, and metals. The structure, size, and composition of these particles can be easily altered in a controllable way to tailor their magnetic, mechanical, thermal, electrical, electro-optical, and catalytic properties.[3–10] The core–shell morphology can be used as a precursor form to produce hollow spheres[11] or to lower the cost of precious materials by coating them on inexpensive cores.[12,13] Core–shell materials can also be used as fluorescent diagnostic labels[14–16] and for avoiding photodegradation,[17,8] enhancing photoluminescence,[14,19,20] creating photonic crystals,[21,22] and obtaining novel optical effects.[23,24] Core–shell particles have been synthesized using metals, semiconductors metal oxides, alloys, dyes, biomolecules, etc. Different schemes for obtaining core–shell particles and their applications have been discussed in literatures.[25,26] Up to now, many methods have been employed to fabricate such core–shell materials, such as sol–gel process,[3] layer-by-layer technique,[27] template directed self-assembly,[28] and encapsulation of silica nanoparticles by *in situ* polymerization.[29]

The demand for high-resolution and increased efficiency in phosphors for cathode ray tubes (CRT) and field emissive displays (FEDs) has promoted the development of phosphors that perform at low voltages.[30] In particular, phosphors made up of small, ideally spherical particles are of interest because they offer the possibility of brighter cathodoluminescent performance, high definition, and much improved screen packing.[31] The ideal morphology of phosphor particles includes a perfect spherical (<3 μm) shape, narrow size distribution, and non-agglomeration. Spherical morphology of the phosphors is good for high brightness and high resolution. Additionally, high packing

*Author to whom correspondence should be addressed.

1533-4880/2006/6/1416/007 doi:10.1166/jnn.2006.195

densities and low scattering of light can also be obtained by using spherical phosphors. Nowadays, many synthetic routes have been developed to control the size and distribution of phosphor particles, such as spray pyrolysis[32] and fluxes precipitation.[33]

Silica can be easily fabricated controllably in spherical morphology from nanometer- to micronmeter size.[34] If the silica spheres are coated with layers of phosphors, a kind of core–shell phosphor materials with spherical morphology will be obtained, and the size for the phosphor particles can be controlled by the silica cores. Furthermore, because silica is cheaper than most of the phosphor materials (which often employ the expensive rare earth elements as the activators and/or host components), the core–shell phosphor materials will be cheaper than the pure phosphor materials in unit mass. It would be of great interest and importance that the phosphor layers can be prepared on silica glass substrates and silica spheres via a sol–gel process.[35, 36] Many of the rare earth oxides are very expensive and this has limited their use in a number of applications. The europium-doped Gd_2O_3 phosphors have been paid much attention in terms of their luminescence properties as a red-emitting phosphor.[37, 38] Combining the promising fluorescent properties of Gd_2O_3:Eu^{3+} with nanoparticles in the form of coatings or thin films on the inert cores is important for the fabrication of the cost efficient phosphors.[39] In this paper we report an alternative sol–gel synthesis of the SiO_2@Gd_2O_3:Eu^{3+} core–shell structured phosphor particles, and characterize the structure, morphology, and photoluminescent properties in details.

2. EXPERIMENTAL DETAILS

2.1. Synthesis of Silica Cores

Amorphous submicron spheres of silica in the size range of 500–600 nm were synthesized by the well known Stöber process, i.e., the hydrolysis of TEOS in an ethanol solution containing water and ammonia.[34] This method yielded the colloidal solution of silica particles with a narrow size distribution in submicron range, and the particle size of silica depended on relative concentration of the reactants. In a typical experiment, the mixture containing 21 mL of TEOS (99 wt%, analytical reagent, A. R.), 9 mL of deionized H_2O, and 245 mL of NH_4OH (25 wt%, A. R.) were added into 225 mL of absolute ethanol and stirred at room temperature for 4 h, resulting in the formation of white silica colloidal suspension. The silica particles were centrifugally separated from the suspension and washed with ethanol four times.

2.2. Coating of SiO_2 Cores with Gd_2O_3:Eu^{3+} Shells

SiO_2 core/Gd_2O_3:Eu^{3+} shell particles (SiO_2@Gd_2O_3:Eu^{3+}) were prepared by a Pechini sol–gel process.[35, 36, 40] The doping concentration of Eu^{3+} was 5 mol% that of Gd^{3+} in Gd_2O_3 host ($Gd_{1.9}Eu_{0.1}O_3$), which had been optimized by us previously.[41] 7.6 mmol Gd_2O_3 (99.99%, Shanghai Yuelong New Materials Co., Ltd.) and 0.4 mmol Eu_2O_3 (99.99%, Shanghai Yuelong New Materials Co., Ltd.) were dissolved in dilute HNO_3 (A. R., Beijing Beihua Chemicals Co., Ltd.) under vigorous stirring, and the superfluous HNO_3 was driven off until the pH value of the solution reached between two and three. Then 30 mL

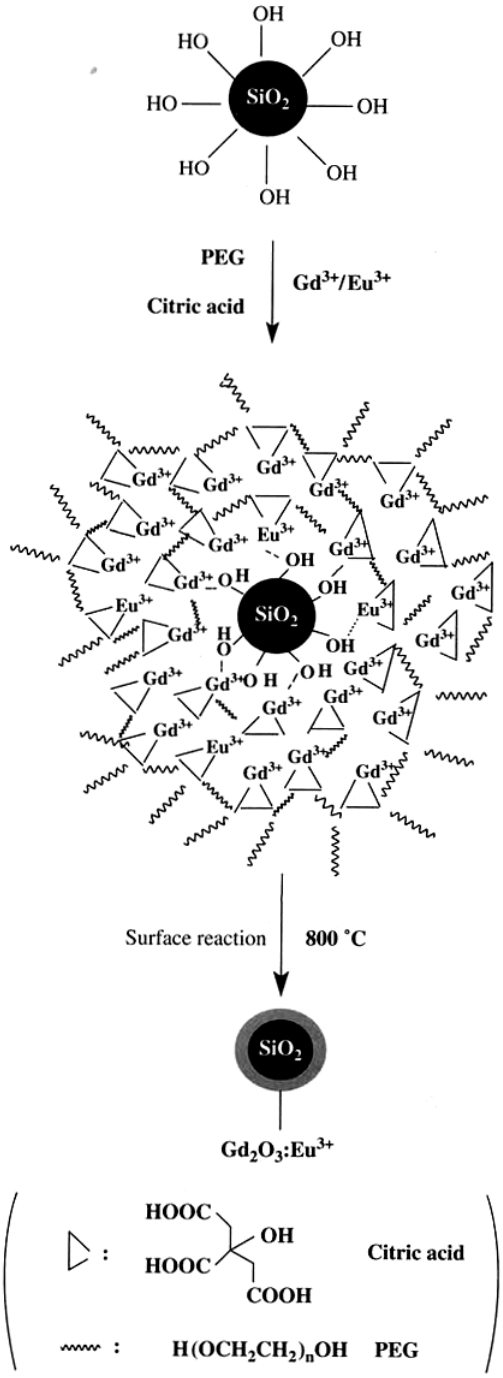

Scheme 1. Formation process of SiO_2@Gd_2O_3:Eu^{3+} core–shell particles.

water–ethanol (v/v = 1:7) solution containing 32 mmol citric acid (A. R., Beijing Beihua Chemicals Co., Ltd.) as chelating agent for the metal ions was added to the above solution. The resulted molar concentrations for Gd^{3+} and Eu^{3+} ions are 0.5067 mol/L and 0.0267 mol/L, respectively. Then 0.48 mmol polyethylene glycol (PEG, molecular weight = 10000, A. R., Beijing Beihua Chemicals Co., Ltd.) was added as a cross-linking agent. Highly transparent sols were obtained after stirring for a few hours, and then 50 mmol silica particles were added under stirring. The final molar ratio of SiO_2/Gd^{3+} was 3.3. The suspension was further stirred for another 3 h, and then the particles were separated by centrifugation. The particle samples were dried at 100 °C for 1 h and then annealed to the desired temperature (300–800 °C) with a heating rate of 1 °C/min and held there for 2 h in air. The above process was repeated for several times to increase the thickness of the Gd_2O_3:Eu^{3+} shells. In this way, the core–shell structured SiO_2@Gd_2O_3:Eu^{3+} materials had been obtained, and the whole process was shown in Scheme 1. For the purpose of comparison, the coating sol was evaporated to form powders, which were annealed in a similar process to produce the pure Gd_2O_3:Eu^{3+} powder phosphors.

2.3. Characterization

The X-ray diffraction (XRD) of the powder samples was examined on a Rigaku-Dmax 2500 diffractometer using Cu Kα radiation ($\lambda = 0.15405$ nm). FT-IR spectra were measured with Perking-Elmer 580B infrared spectrophotometer with the KBr pellet technique. The morphology of samples was inspected using a field emission scanning electron microscope (XL30, Philips) and transmission electron microscope (JEOL-2010, 200 kV). The excitation and emission spectra were taken on a Hitachi F-4500 spectrofluorimeter equipped with a 150 W xenon lamp as the excitation source. Luminescence decay curves were obtained from a Lecroy Wave Runner 6100 Digital Oscilloscope (1 GHz) using 253 nm laser (pulse width = 4 ns, gate = 50 ns) as the excitation source (Continuum Sunlite OPO). All the measurements were performed at room temperature (RT).

3. RESULTS AND DISCUSSION

3.1. Formation and Morphology of SiO_2@Gd_2O_3:Eu^{3+} Core–Shell Nanoparticles

Figure 1 shows the X-ray diffraction patterns of SiO_2 @Gd_2O_3:Eu^{3+} core–shell samples annealed at different temperatures (300–800 °C: a–f), bare SiO_2 particles annealed at 800 °C (g), pure Gd_2O_3:Eu^{3+} powder (h), as well as the JCPDS card (No. 12-797) for Gd_2O_3 (i). For SiO_2@Gd_2O_3:Eu^{3+} core–shell sample annealed at 300 °C (Fig. 1a), no diffraction peak is observed except for a broad band centered at $2\theta = 22.00°$ (characteristic peak

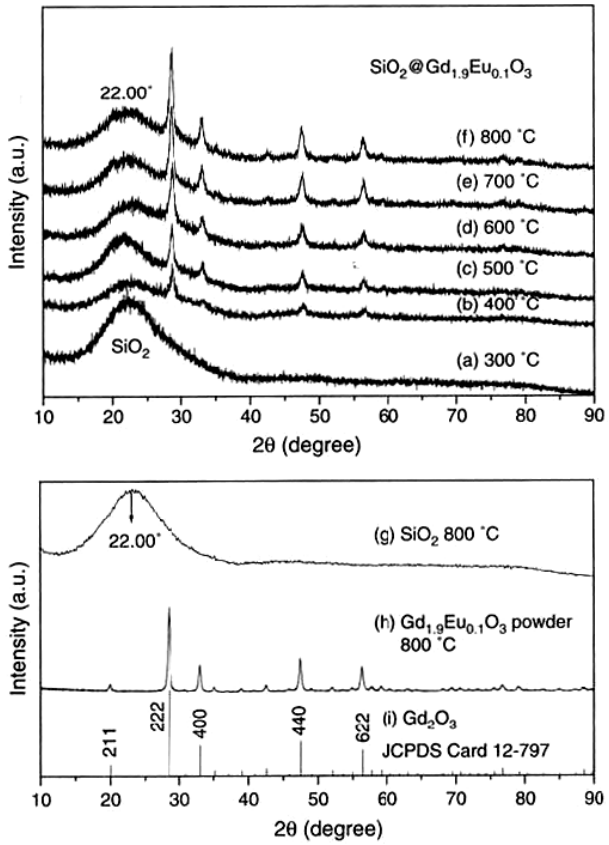

Fig. 1. X-ray diffraction patterns of SiO_2@Gd_2O_3:Eu^{3+} core–shell samples annealed at different temperatures (300–800 °C: a–f), bare SiO_2 particles annealed at 800 °C (g), pure Gd_2O_3:Eu^{3+} powder (h), as well as the JCPDS card (No. 12-797) for Gd_2O_3 (i).

for amorphous SiO_2, JCPDS 29-0085), which is similar to that of the bare SiO_2 particles annealed at 800 °C (Fig. 1g). This indicates that the crystalline shell of Gd_2O_3:Eu^{3+} has not formed at this low annealing temperature. After annealing at 400 °C, crystalline Gd_2O_3:Eu^{3+} can be observed on SiO_2@Gd_2O_3:Eu^{3+} core–shell sample (Fig. 1b). The crystallinity of Gd_2O_3:Eu^{3+} on the core–shell particles increases with raising the annealing temperature (Figs. 1c–f). All the diffraction peaks for SiO_2@Gd_2O_3:Eu^{3+} core–shell samples are in good agreement with those of pure Gd_2O_3:Eu^{3+} powder sample annealed at 800 °C (Fig. 1h) and the standard diffraction data for crystalline Gd_2O_3 (Fig. 1i, JCPDS card No. 12-797). Note that the characteristic amorphous band (22.00 °C) of SiO_2 can be observed for all the SiO_2@Gd_2O_3:Eu^{3+} core–shell samples annealed from 300 to 800 °C besides the diffraction peaks due to Gd_2O_3. No diffraction peak due to other phase is detected, indicating that no reaction has occurred between the SiO_2 cores and Gd_2O_3:Eu^{3+} shells when the annealing temperature is lower than 800 °C.

The FT-IR spectra of the as formed SiO_2, 800 °C annealed SiO_2@Gd_2O_3:Eu^{3+} core–shell sample and pure Gd_2O_3:Eu^{3+} powders are shown in Figures 2(a), (b),

RESEARCH ARTICLE

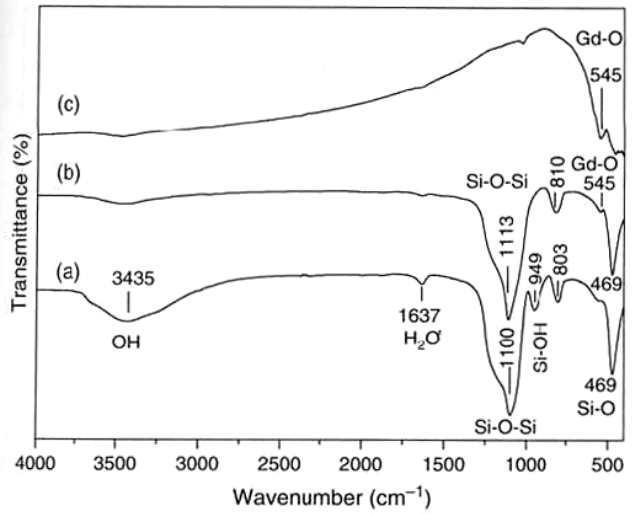

Fig. 2. FT-IR spectra of the as formed SiO_2 (a), SiO_2@Gd_2O_3:Eu^{3+} core–shell samples (b), and Gd_2O_3:Eu^{3+} powder (c) annealed at 800 °C.

and (c) respectively. In Figure 2(a) for the as formed SiO_2 particles, the absorption bands due to OH (3435 cm^{-1}), H_2O (1637 cm^{-1}), Si–O–Si (ν_{as}, 1100 cm^{-1}; ν_s, 803 cm^{-1}), Si–OH (ν_s, 949 cm^{-1}), and Si–O (δ, 469 cm^{-1}) bonds (where ν_{as} = asymmetric stretching, ν_s = symmetric stretching, δ = bending) are observed.[42] This indicates that the as formed SiO_2 particles contain a large amount of OH groups and H_2O on their surfaces.[6] The surface Si–OH groups play an important role for bonding the metal ions (Gd^{3+}, Eu^{3+}) from the coating sol and forming the Gd_2O_3:Eu^{3+} layers on the SiO_2 surfaces in the following annealing process,[36, 43] as shown in Scheme 1. In the Pechini process, the citric acid first formed chelate complexes with Gd^{3+} and Eu^{3+}, then the left carboxylic acid groups in the citric acid reacted with polyethylene glycol to form polyester with a suitable viscosity. The Gd^{3+} and Eu^{3+}, stabilized by the chelating and polymerizing process, were homogeneously distributed in the solution. By stirring silica particles in the solution, a lot of Gd^{3+} and Eu^{3+} were absorbed onto the silica particles by physical and chemical interactions. After drying and annealing process, the Gd^{3+} and Eu^{3+}-complexes decomposed to form Gd_2O_3:Eu^{3+} layer on the silica cores.[44] For pure Gd_2O_3:Eu^{3+} powders (Fig. 2c), the weak peak at 545 cm^{-1} is attributed to the absorption of Gd (Eu)–O bonds.[45] In Figure 2(b) for the SiO_2@Gd_2O_3:Eu^{3+} core–shell sample the characteristic absorption peaks of Gd–O bond (545 cm^{-1}), and Si–O–Si bond (1114 cm^{-1}; 803 cm^{-1}), Si–O bond (469 cm^{-1}) for amorphous SiO_2 (Fig. 2a) have been observed clearly. This suggests that crystalline phase of Gd_2O_3 has formed after annealing at 800 °C, agreeing well with the results of XRD. The signal of OH groups from the as formed silica particles have almost disappeared for Gd_2O_3:Eu^{3+}@SiO_2 core–shell particles annealed at 800 °C. These results are consistent with those of XRD, and further demonstrate the formation of

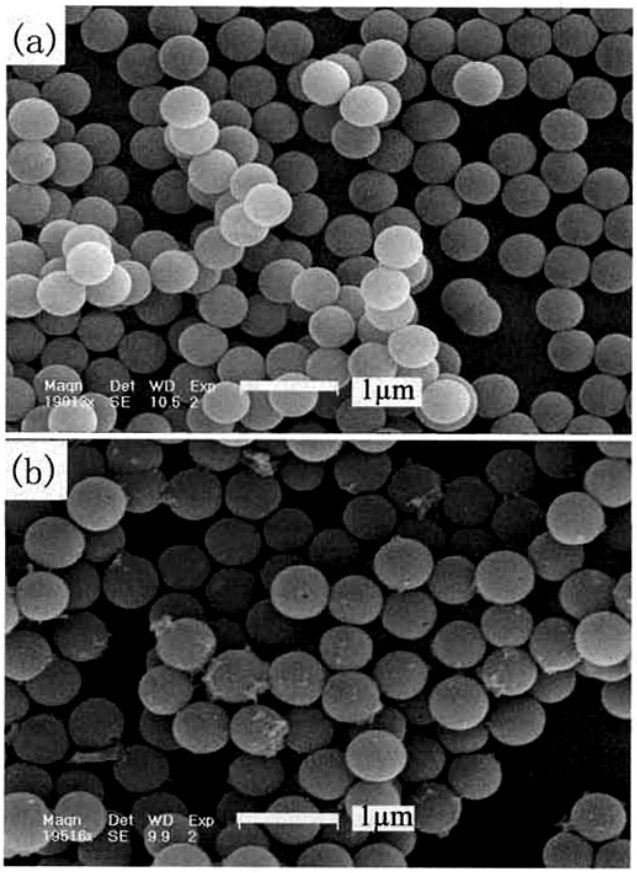

Fig. 3. FESEM micrographs of the as formed SiO_2 (a) and the SiO_2 particles coated with three layers of Gd_2O_3:Eu^{3+} (b) annealed at 800 °C.

crystalline Gd_2O_3:Eu^{3+} coatings on the silica surfaces via the sol–gel deposition and annealing process.

Figure 3 shows the SEM micrographs of the as formed SiO_2 particles (a) and SiO_2 particles coated by three layers of Gd_2O_3:Eu^{3+} (b), respectively. From the SEM micrograph of Figure 3(a) we can observe that the as formed SiO_2 consists of spherical particles with an average size of 500 nm, and these particles are non-aggregated with narrow size distribution. After functionalizing the silica particles by Gd_2O_3:Eu^{3+} coatings, the resulted SiO_2@Gd_2O_3:Eu^{3+} particles still keep the morphological properties of the silica particles, i.e., these particles are still spherical and non-aggregated, but slightly larger than the pure silica particles due to the additional layers of Gd_2O_3:Eu^{3+} on them, as shown in Figure 3(b). Moreover, the surface of the SiO_2@Gd_2O_3:Eu^{3+} particles is not as smooth as that of bare SiO_2 particles (there is certain amount of non-spherical clusters apparently stuck on the surface of the coated particles, and they may be attributed to the clusters of Gd_2O_3:Eu^{3+}), also indicating that the Gd_2O_3:Eu^{3+} materials have been coated on the surfaces of silica particles by our experimental process. It should be mentioned that the SEM micrographs can only provide the general information on the morphology of SiO_2@Gd_2O_3:Eu^{3+} particles in large scale (namely, all

RESEARCH ARTICLE

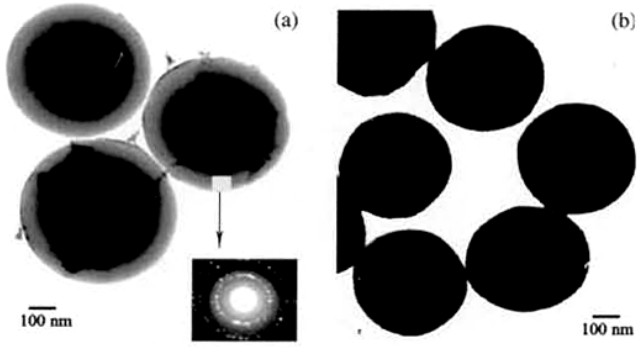

Fig. 4. TEM micrographs of the SiO_2 coated with three layers of Gd_2O_3:Eu^{3+} (a) and the bare SiO_2 particles (b) annealed at 800 °C. The inset in (a) is electron diffraction pattern for the selective region as indicated.

of the SiO_2 particles remain spherical and non-aggregated subjected to the sol–gel coating of Gd_2O_3:Eu^{3+} layers on them) and the core–shell structure of SiO_2@Gd_2O_3:Eu^{3+} particles can not be resolved from the SEM micrographs due to the low magnification.

The core–shell structure of SiO_2@Gd_2O_3:Eu^{3+} particles can be observed clearly by the TEM images. Representative TEM micrographs for the SiO_2 particles coated by three layers of Gd_2O_3:Eu^{3+} as well as for the pure SiO_2 particles (as reference) are shown in Figures 4(a) and (b), respectively. In Figure 4(a), the core-shell structure for the SiO_2@Gd_2O_3:Eu^{3+} particles can be seen clearly due to the different electron penetrability for the cores and shells. The cores are black spheres with an average size of 500 nm (similar to the pure SiO_2 particles in Fig. 4b), and the shells have gray color with an average thickness of 70 nm. The electron diffraction measurement was performed in the interface region of the core and shell of a particle as labeled in Figure 4(a), and the electron diffraction rings in Figure 4 (a, inset) demonstrate the presence of crystalline phase (Gd_2O_3:Eu^{3+}) on the surface of the core–shell particles.

3.2. Photoluminescence Properties

Upon UV excitation, the SiO_2@Gd_2O_3:Eu^{3+} core–shell phosphors exhibit strong red luminescence. Figure 5(a) and (b) show the excitation and emission spectra for SiO_2@Gd_2O_3:Eu^{3+} core–shell phosphors respectively. The excitation spectrum was obtained by monitoring the emission of Eu^{3+} $^5D_0$–$^7F_2$ transition at 610 nm. It can be seen clearly that the excitation spectrum consists of an intense double band peaking around 250 nm and 232 nm. The former (around 250 nm can be attributed to the charge transfer band (CTB) between O^{2-} and Eu^{3+}, and the latter (232 nm) to the Gd_2O_3 host excitation band.[41] The sharp peak at 253 nm superimposed on the CTB of Eu^{3+} and the weak shoulder at 277 nm can be attributed to the ^8S–^6D and ^8S–^6I transition lines of Gd^{3+}, respectively.[46] The general f–f transition lines of Eu^{3+} can be observed in

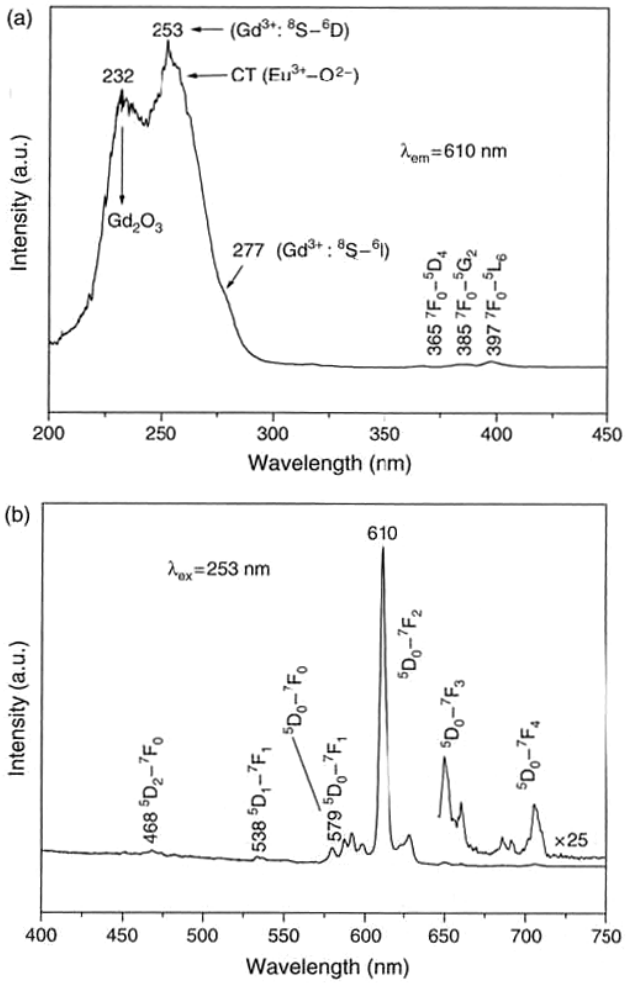

Fig. 5. Excitation (a) and emission (b) spectra of SiO_2@Gd_2O_3:Eu^{3+} core–shell particles annealed at 800 °C.

the longer wavelength region (366 nm: $^7F_0$–$^5D_4$; 385 nm: $^7F_0$–$^5G_2$; 397 nm: $^7F_0$–$^5L_6$) with very weak intensity. The presence of Gd_2O_3 host band and Gd^{3+} excitation lines in the excitation spectrum of Eu^{3+} indicates that there exists an efficient energy transfer from Gd_2O_3 host and Gd^{3+} to the doped Eu^{3+}. Excitation with 253 nm UV (into CTB of Eu^{3+}–O^{2-} together with Gd^{3+}) yields the emission spectrum corresponding to f–f transitions of Eu^{3+} $^5D_{0,1,2,}$–^7F_J (J = 0, 1, 2, 3, 4, Fig. 5b), which is dominated by the hypersensitive red emission $^5D_0$–$^7F_2$ transition at 610 nm. Other observed transition lines for Eu^{3+} are labeled in the figure. The emission spectrum of SiO_2@Gd_2O_3:Eu^{3+} core–shell phosphors agrees well with those of Gd_2O_3:Eu^{3+} film and powder reported previously and can be explained in a similar way as before.[41, 47–49]

The presence of emission lines from higher excited states of Eu^{3+} ($^5D_1$, $^5D_2$) is attributed to the low vibration energy of Gd–O bond (545 cm^{-1}). The multiphonon relaxation by Gd–O vibration is not able to bridge the gaps between the higher energy levels ($^5D_1$, $^5D_2$) and $^5D_0$ level of Eu^{3+} completely, resulting in the emissions from these levels.[46]

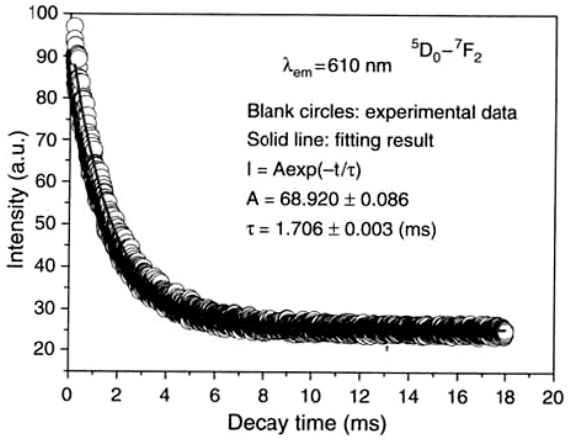

Fig. 6. The decay curve for the $^5D_0$–$^7F_2$ (610 nm) emission of Eu^{3+} in SiO_2@Gd_2O_3:Eu^{3+} sample annealed at 800 °C.

The representative decay curve for the luminescence of Eu^{3+} ion $^5D_0$–$^7F_2$ (610 nm) in the SiO_2@Gd_2O_3:Eu^{3+} core–shell phosphors annealed at 800 °C is shown in Figure 6. The decay curve can be well fitted into single exponential function as $I = A\exp(-t/\tau)$, (where τ is the $1/e$ lifetime of the rare earth ion) and the fitting parameters are shown inside Figure 6. A lifetime (τ) of 1.706 ms is obtained for $^5D_0$–$^7F_2$ (610 nm) emission of Eu^{3+} in SiO_2@Gd_2O_3:Eu^{3+} sample.

The PL emission intensity of the Eu^{3+} in SiO_2@Gd_2O_3:Eu^{3+} core–shell phosphors is affected by annealing temperatures. Figure 7 shows the effect of annealing temperatures on the PL intensities. It can be seen that the PL intensity increases with the increasing of annealing temperatures from 400 to 800 °C. This is because with the increase of annealing temperature the content of impurities in the SiO_2@Gd_2O_3:Eu^{3+} core–shell phosphors such as −OH, NO_3^-, −OR, $-CH_2$ and others decreases and the crystallinity of Gd_2O_3:Eu^{3+} shell increases. The quenching of the luminescence of the Eu^{3+} by the vibrations of these impurities decreases, resulting in the increase of their lifetimes and PL emission intensity.[35, 36]

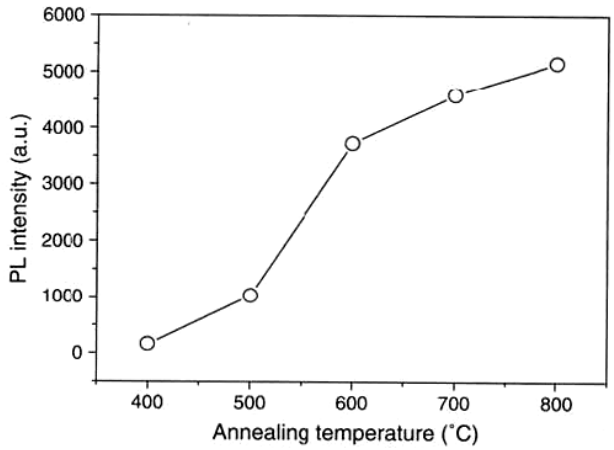

Fig. 7. The PL emission intensity of Eu^{3+} in SiO_2@Gd_2O_3:Eu^{3+} sample as a function of annealing temperatures.

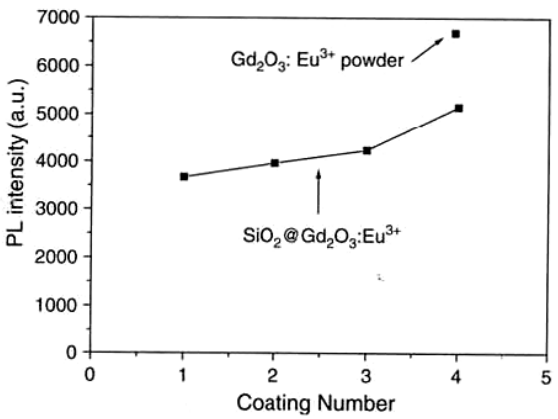

Fig. 8. The PL emission intensity of Eu^{3+} as a function of the number of coatings (N) of Gd_2O_3:Eu^{3+} on SiO_2 particles. The PL intensity of pure Gd_2O_3:Eu^{3+} powder is also given for comparison.

Coating number is also an important factor influencing PL intensity. Figure 8 shows the effect of coating number on the PL intensity of SiO_2@Gd_2O_3:Eu^{3+} core–shell phosphors annealed at the same temperature. The PL intensity increases with the increasing of the coating number, which is due to the increase of the thickness of Gd_2O_3:Eu^{3+} shells on the SiO_2 spheres. When the coating number is four times, the PL intensity is about 77% of that of pure Gd_2O_3:Eu^{3+} powders, as shown in Figure 8.[36]

4. CONCLUSIONS

Nanocrystalline SiO_2@Gd_2O_3:Eu^{3+} core–shell phosphors were successfully prepared by the Pechini sol–gel process using the cheap and non-toxic inorganic compounds as main precursors. The obtained SiO_2@Gd_2O_3:Eu^{3+} core–shell phosphors have spherical morphology, submicron size, and narrow size distribution. The PL intensity of the core–shell phosphors can be tuned by the annealing temperature and the number of coatings. With the increase of annealing temperature and the number of coatings, the PL intensity increases. The current method can be extended to prepare various other core–shell phosphors with homogeneous morphology and decrease the cost of phosphors to some degree.

Acknowledgments: This project is financially supported by the foundation of "Bairen Jihua" of Chinese Academy of Sciences, the National Natural Science Foundation of China (50225205, 50572103, 20431030) and the MOST of China (No. 2003CB314707). Dr M. Yu is grateful for the special starting research fund for the Awardees of President Prize of Chinese Academy of Sciences (2005–2007). Prof. J. Fang is grateful for the financial support by the foundation of a two-base program for international cooperation of NSFC (00310530) related to Project 50225205, and NSF DMR-0449580.

References and Notes

1. R. C. Plaza, J. D. G. Duran, and A. Quirantes, *J. Coll. Interf. Sci.* 194, 398 (**1997**).
2. A. Rogach, A. Susha, F. Caruso, G. Sukhorukov, A. Kornowski, S. Kershaw, H. Mohwald, A. Eychmuller, and H. Weller, *Adv. Mater.* 12, 333 (**2000**).
3. R. A. Caruso and M. Antonietti, *Chem. Mater.* 13, 3272 (**2001**).
4. F. Caruso, M. Spasova, and V. Salgueirno-Maceria, *Adv. Mater.* 13, 1090 (**2001**).
5. Z. H. Jiang and C. Y. Liu, *J. Phys. Chem. B* 107, 12411 (**2003**).
6. H. Sertchook and D. Avnir, *Chem. Mater.* 15, 1690 (**2003**).
7. M. Giersig, T. Ung, L. M. Liz-Marzan, and P. Mulvaney, *Adv. Mater.* 9, 570 (**1997**).
8. T. Ung, L. M. Liz-Marzan, and P. Mulvaney, *Langmuir* 14, 3740 (**1998**).
9. S. J. Oldenburg, R. D. Averitt, S. L. Westcott, and N. J. Halas, *Chem. Phys. Lett.* 188, 243 (**1998**).
10. M. S. Fleming, T. K. Mandal, and D. R. Walt, *Chem. Mater.* 13, 2210 (**2001**).
11. Z. Y. Zhong, Y. D. Yin, B. Gates, and Y. N. Xia, *Adv. Mater.* 12, 206 (**2000**).
12. M. Ocana, W. P. Hsu, and E. Matijevic, *Langmuir* 7, 2911 (**1991**).
13. W. P. Hsu, R. C. Yu, and E. Matijevic, *J. Coll. Interf. Sci.* 156, 56 (**1993**).
14. M. Bruchez, M. Moronne, P. Gin, S. Weiss, and A. P. Alivisatos, *Science* 281, 2013 (**1998**).
15. O. V. Makarova, A. E. Ostafin, H. Miyoshi, J. R. Norris, Jr., and D. Meisel, *J. Phys. Chem. B* 103, 9080 (**1999**).
16. B. J. Battersby, D. Bryant, W. Meutermans, D. Matthews, M. L. Smythe, and M. Trau, *J. Am. Chem. Soc.* 122, 2138 (**2000**).
17. M. A. Correa-Durate, M. Giersig, and L. M. Liz-Marzan, *Chem. Phys. Lett.* 286, 497 (**1998**).
18. R. Tapec, X. Zhao, and W. Tan, *J. Nanosci. Nanotechnol.* 2, 40 (**2002**).
19. B. O. Dabbousi, J. Rodriguez-Viejo, F. V. Mikulec, R. R. Heine, H. Mattoussi, R. Ober, K. F. Jensen, and M. G. Bawendi, *J. Phys. Chem. B* 101, 9463 (**1997**).
20. A. S. Ethiraj, N. Hebalkar, S. K. Kulkarni, R. Pascricha, C. Dem, M. Schmitt, W. Kiefer, L. Weinhardt, S. Joshi, R. Fink, C. Heske, C. Kumpf, and E. Umbach, *J. Chem. Phys.* 118, 8945 (**2003**).
21. K. P. Velikov, A. Moroz, and A. van Blaaderen, *Appl. Phys. Lett.* 80, 49 (**2002**).
22. M. Alijandro-Arellano, A. Blanco, T. Ung, P. Mulvaney, and L. M. Liz-Marzan, *Pure Appl. Chem.* 72, 257 (**2002**).
23. S. J. Oldenberg, R. D. Averitt, S. L. Westcott, and N. J. Halas, *Chem. Phys. Lett.* 288, 257 (**2000**).
24. L. M. Liz-Marzan, M. Giersig, and P. Mulvaney, *Langmuir* 12, 4329 (**1996**).
25. F. Caruso, *Adv. Mater.* 13, 11 (**2000**).
26. L. M. Liz-Marzan, M. A. Correa-Durate, I. Pastorza-Santos, P. Mulvaney, T. Ung, M. Giersig, and N. A. Kotov, in Handbook of Surfaces and Interfaces of Materials, edited by H. S. Nalwa, Academic Press, San Diego (**2001**), Vol. 3, p. 189.
27. P. Schuetzand and F. Caruso, *Chem. Mater.* 14, 4509 (**2002**).
28. S. R. Hall, S. A. Davis, and S. Mann, *Langmuir* 16, 1454 (**2000**).
29. I. Sondi, T. H. Fedynyshyn, R. Sinta, and E. Matijevic, *Langmuir* 16, 9031 (**2000**).
30. M. I. Martinez-Rubio, T. G. Ireland, G. R. Fern, J. Silver, and M. J. Snowden, *Langmuir* 17, 7145 (**2001**).
31. Y. D. Jiang, Z. L. Wang, F. Zhang, H. G. Paris, and C. J. Summers, *J. Mater. Res.* 13, 2950 (**1998**).
32. K. Y. Jung, D. Y. Lee, Y. C. Kang, and H. D. Park, *J. Lumin.* 105, 127 (**2003**).
33. A. Celikkaya and M. Akinc, *J. Am. Ceram. Soc.* 73, 2360 (**1990**).
34. W. Stöber, A. Fink, and E. Bohn, *J. Coll. Interf. Sci.* 26, 62 (**1968**).
35. M. Yu, J. Lin, Z. Wang, J. Fu, S. Wang, H. J. Zhang, and Y. C. Han, *Chem. Mater.* 14, 2224 (**2002**).
36. M. Yu, J. Lin, and J. Fang, *Chem. Mater.* 17, 1783 (**2005**).
37. J. C. Park, H. K. Moon, D. K. Kim, S. H. Byeon, B. C. Kim, and K. S. Suh, *Appl. Phys. Lett.* 77, 2162 (**2000**).
38. Y. C. Kang, S. B. Park, I. W. Lenggoro, and K. Okuyama, *J. Phys. Chem. Solids* 60, 379 (**1999**).
39. G. X. Liu, G. Y. Hong, and D. X. Sun, *J. Coll. Interf. Sci.* 278, 133 (**2004**).
40. M. P. Pechini, U.S. Patent 3 330 697 (**1967**).
41. M. L. Pang, J. Lin, J. Fu, R. B. Xing, C. X. Luo, and Y. C. Han, *Opt. Mater.* 23, 547 (**2003**).
42. Y. Chen and J. O. Iroh, *Chem. Mater.* 11, 1218 (**1999**).
43. H. Giesche and E. Matijević, *J. Mater. Res.* 9, 436 (**1994**).
44. D. Y. Kong, M. Yu, C. K. Lin, X. M. Liu, J. Lin, and J. Fang, *J. Electrochem. Soc.* 152, H146 (**2005**).
45. A. Garcia-Murillo, C. L. Luyer, C. Dujardin, C. Pedrini, and J. Mugnier, *Opt. Mater.* 16, 39 (**2001**).
46. G. Blasse and B. C. Grabmaier, *Luminescent Materials*, Springer-Verlag, Berlin (**1994**).
47. S. Yeon Seo, K. S. Sohn, H. D. Park, and S. Lee, *J. Electrochem. Soc.* 149, H12 (**2002**).
48. M. A. Lim, Y. C. Kang, and H. D. Park, *J. Electrochem. Soc.* 148, H171 (**2001**).
49. R. Bazzi, M. A. Flores, C. Louis, K. Lebbou, W. Zhang, C. Dujardin, S. Roux, B. Mercier, G. Ledoux, E. Bernstein, P. Perriat, and O. Tillement, *J. Coll. Interf. Sci.* 273, 191 (**2004**).

Received: 7 October 2005. Revised/Accepted: 7 February 2006.

RESEARCH ARTICLE